# Viscoelasticity of the human red blood cell

**Marina Puig-de-Morales-Marinkovic, Kevin T. Turner, James P. Butler, Jeffrey J. Fredberg and Subra Suresh**

*Am J Physiol Cell Physiol* 293:597-605, 2007. First published Apr 11, 2007;
doi:10.1152/ajpcell.00562.2006

*Am J Physiol Cell Physiol* 293: C597–C605, 2007.
First published April 11, 2007; doi:10.1152/ajpcell.00562.2006.

# Viscoelasticity of the human red blood cell

**Marina Puig-de-Morales-Marinkovic,[1]* Kevin T. Turner,[2,3]* James P. Butler,[1] Jeffrey J. Fredberg,[1] and Subra Suresh[2,4]**

[1]*Department of Environmental Health, Harvard School of Public Health, Boston;* [2]*Department of Materials Science and Engineering, Massachusetts Institute of Technology, Cambridge, Massachusetts;* [3]*Department of Mechanical Engineering, University of Wisconsin-Madison, Madison, Wisconsin; and* [4]*Department of Biological Engineering, Massachusetts Institute of Technology, Cambridge, Massachusetts*

Submitted 7 November 2006; accepted in final form 7 April 2007

**Puig-De-Morales-Marinkovic M, Turner KT, Butler JP, Fredberg JJ, Suresh S.** Viscoelasticity of the human red blood cell. *Am J Physiol Cell Physiol* 293: C597–C605, 2007. First published April 11, 2007; doi:10.1152/ajpcell.00562.2006.—We report here the first measurements of the complex modulus of the isolated red blood cell (RBC). Because the RBC is often larger than capillary diameter, important determinants of microcirculatory function are RBC deformability and its changes with pathologies, such as sickle cell disease and malaria. A functionalized ferrimagnetic microbead was attached to the membrane of healthy RBC and then subjected to an oscillatory magnetic field. The resulting torque caused cell deformation. From the oscillatory forcing and resulting bead motions, which were tracked optically, we computed elastic and frictional moduli, $g'$ and $g''$, respectively, from 0.1 to 100 Hz. The $g'$ was nearly frequency independent and dominated the response at all but the highest frequencies measured. Over three frequency decades, $g''$ increased as a power law with an exponent of 0.64, a result not predicted by any simple model. These data suggest that RBC relaxation times that have been reported previously, and any models that rest upon them, are artifactual; the artifact, we suggest, arises from forcing to an exponential fit data of limited temporal duration. A linear range of response was observed, but, as forcing amplitude increased, nonlinearities became clearly apparent. A finite element model suggests that membrane bending was localized to the vicinity of the bead and dominated membrane shear. While the mechanisms accounting for these RBC dynamics remain unclear, methods described here establish new avenues for the exploration of connections among the mechanical, chemical, and biological characteristics of the RBC in health and disease.

storage modulus; loss modulus; magnetic twisting cytometry; erythrocyte; viscoelasticity; rheology

THE DIAMETER OF A RED BLOOD cell (RBC) is larger than that of the capillary through which it flows in transit through the microcirculation. As such, changes in cell deformability, as occur in malaria (35, 44) and sickle cell disease (39), have the potential to compromise microcirculatory function. To better understand the dynamics of cell deformation in vivo, the nature of the deformability of the RBC must be better characterized.

Knowledge of RBC deformability has come from measurements on populations of cells as well as single-cell tests. Single-cell measurements include micropipette aspiration (MA), optical tweezers (OT), and high-frequency electrical deformation (ED) tests, which apply quasi-static loads and can achieve large deformations (6, 8, 12, 29). These tests have characterized the deformability of the RBC in terms of the shear, bending, and area expansion moduli of the cell membrane, as well as relaxation times. However, little is known about the mechanical properties of the RBC and its associated response to time-dependent loads. Few measurements of the viscoelastic storage and loss moduli of RBCs have been done on cell suspensions (11, 42), but no measurements of these moduli have yet been obtained at the single-cell level.

Here we used optical magnetic twisting cytometry (MTC) to apply direct mechanical loading on the isolated RBC. By applying a torque to a ferrimagnetic microbead tightly bound to the cell surface, the loading was manipulated in a precisely controlled manner. Using this approach, we studied responses to step and sinusoidal loadings. From these measurements, we determined elastic (storage) and frictional (loss) moduli of the single, isolated RBC over wide ranges of forcing time scale and forcing amplitude. We found unexpected dependencies of storage and loss moduli upon frequency that are inconsistent with previous models incorporating discrete relaxation times. Moreover, a finite element (FE) model of static deformations suggests that, in the experiments, membrane bending dominated membrane shear. While mechanisms accounting for RBC dynamics remain unclear, methods described here open new windows into the study of connections among the mechanical, chemical, and biological characteristics of the RBC in health and in disease.

## MATERIALS AND METHODS

*Reagents.* Concanavalin A (ConA), poly-L-lysine, glutaraldehyde, sodium cacodylate buffer, and hexamethyldisilazane (HMDS) were purchased from Sigma (St. Louis, MO). Phosphate-buffered saline (PBS) was purchased from Gibco (Gaithersburg, MD).

*RBC isolation.* RBCs were obtained by drawing ~150 μl of blood from healthy donors by a fingertip needle prick. The blood was diluted in 600 μl of PBS (pH = 7.4) and then washed three times by centrifugation to isolate the RBCs. As the buffer has a physiological osmolarity (~ 270 mosM), the RBCs retain their natural flat, biconcave, disk-like shape.

*Experimental protocols.* Clean, 35-mm glass bottom wells (MatTek, Ashland, MA) were treated with 0.1 mg/ml poly-L-lysine for 1 h at room temperature (T = 22°C). At this concentration, the RBCs adhere firmly to the wells, but retain their biconcave shape (27). RBCs were allowed to adhere for 10 min to the wells, before the beads were added.

* M. Puig-de-Morales-Marinkovic and K. T. Turner contributed equally to this work.

Address for reprint requests and other correspondence: M. Puig-de-Morales Marinkovic, Program in Molecular and Integrative Physiological Sciences (MIPS), Dept. of Environmental Health, Harvard School of Public Health, 665 Huntington Ave., Boston, MA 02115 (e-mail: mpuigdem@hsph.harvard.edu).

The costs of publication of this article were defrayed in part by the payment of page charges. The article must therefore be hereby marked "*advertisement*" in accordance with 18 U.S.C. Section 1734 solely to indicate this fact.

  

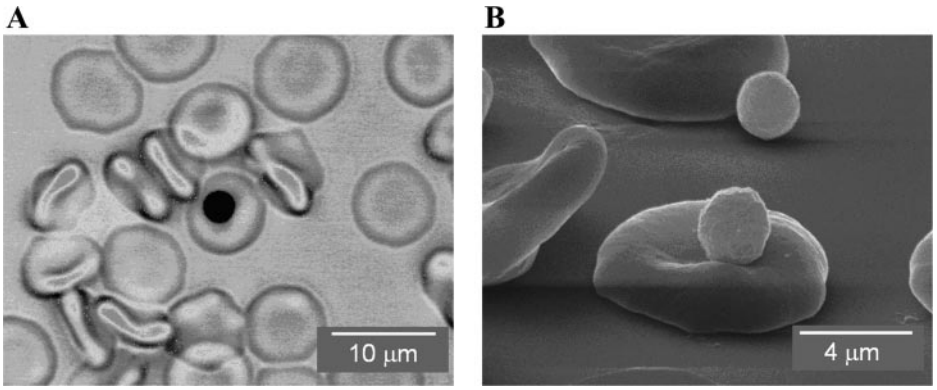


Fig. 1. *A*: red blood cells (RBCs) with beads bound to their surface viewed under bright field with an oil immersion ×63 objective and optically magnified by ×1.5. *B*: scanning electron micrograph of a RBC with a bead bound to the surface. Only cells with individual beads attached near the center of the cell were analyzed. Across all of the tests, the cells had a mean diameter of 8.0 ± 0.6 μm, and the mean distance of the bead from the center of cell was 1.0 ± 0.5 μm.

*Ferrimagnetic microbeads and binding.* Ferrimagnetic beads (solid $Fe_3O_4$, 2.27 μm ± 11.3% diameter) were produced as described previously (18). Beads (1 mg) were coated with ConA by incubating overnight at 4°C in ConA solution (1 mg/ml). ConA is not blood group specific but has an affinity for terminal α-D-mannosyl and α-D-glucosyl residues. A wide variety of serum and membrane glycoproteins have a "core oligosaccharide" structure, which includes α-linked mannose residues, such as band 3. Hence, ConA-coated beads are firmly attached to the spectrin network directly due to the binding through transmembrane glycoproteins and indirectly due to the coupling of the lipid bilayer to the spectrin (37).

Coated beads were rinsed several times in PBS and then added to the RBC preparation in the well. The volume of beads added was controlled such that there was approximately one bead per RBC. The preparation was incubated with the beads for 10 min, allowing adhesion of microbeads to the RBC membrane. Wells were then washed twice with PBS to remove unbound beads and cells. All measurements were made on beads located near the center of the cell (Fig. 1) and were at room temperature.

*Immunoelectron microscopy.* A sample of RBCs with beads attached was fixed by treating with a solution containing 2.5% glutaraldehyde in 0.085 M of sodium cacodylate buffer (G/NaC) for 1 h at room temperature. The cells were washed twice in G/NaC for 5 min each. Fixed cells were then dehydrated through a graded series of ethanol (EtOH) baths for 10 min each: 25, 50, 70, 95, and 100% (three times). Cells were treated with 50:50 HMDS in 100% EtOH for 2 h, followed by treatment with 100% HMDS twice for 30 min. The sample was allowed to air dry overnight and were then sputter coated with a layer of Au in a Hummer V (Anatech, Alexandria, VA). The cells were examined with a 1450VP scanning electron (Carl Zeiss SMT, Thornwood, NY).

*MTC with optical detection.* The experimental setup for MTC with optical detection has been described in detail elsewhere (18, 19). Briefly, after the cells were adhered on the bottom of a glass well and the beads attached, the well was placed on the stage of an inverted microscope (Leica DM IRBE, Leica Microsystems, Weitzler, Germany) and viewed under bright field with an oil immersion ×63 objective and optically magnified ×1.5. Beads were first magnetized horizontally and then subjected to a vertical magnetic field (Fig. 2). This magnetic field induces a specific (mechanical) torque, $T_s(t)$, on the bead.

The $T_s(t)$ is defined as the mechanical torque per unit bead volume and has dimensions of stress, Pa. $T_s(t)$ is given by

$$T_s(t) = c \cdot H \cdot \cos\theta \qquad (1)$$

where $H$ is the applied magnetic twisting field in units of Gauss, θ is the angle of the bead's magnetic moment relative to the original magnetization direction, and $c$ is the bead constant, expressed as torque per unit bead volume per Gauss. The bead constant is determined by placing beads in a fluid of known viscosity and then measuring the angular velocity that results from an applied magnetic field (48). The bead constant in this study was $c = 0.225$ Pa/G. As θ was small, the cos θ term in *Eq. 1* was assumed to be unity when computing the specific torque from the applied magnetic twisting field. This results in errors of <5% for small bead rotations ($\theta < 18°$) or small lateral bead displacements ($d < 450$ nm) in the case of a pivoting motion of the bead around a contact point at the bead perimeter.

The magnetic twisting field creates a torque that acts upon the adherent bead and causes both a rotation and a lateral translation (Fig. 2). The magnitude of the rotation and translation is a function of the magnitude of the applied torque, the geometry of the cell and the bead attachment, and the mechanical properties of the cell. Both rotation and translation result from the loading, because the bead is only attached near its base, and hence the torque applied to the bead is transferred to the cell as a bending moment supported by both normal and tangential tractions. The bead motions were tracked through images captured by a charge-coupled device camera (JAI CV-M10, Gloatrup, Denmark) with an exposure time of 0.1 ms and acquisition frequency of 24 Hz. From recorded images, the bead position $d(t)$ was computed using an intensity-weighted center-of-mass algorithm that provides an accuracy in $d(t)$ of better than 5 nm (19).

*Mechanical tests.* Two types of forcing were used: sinusoidal and step functions. Sinusoidal forcing spanned $10^{-1}$ to $10^2$ Hz and amplitudes from 0.5 to 4 G. As described previously (19), heterodyning was used to sample the displacement response in tests where the

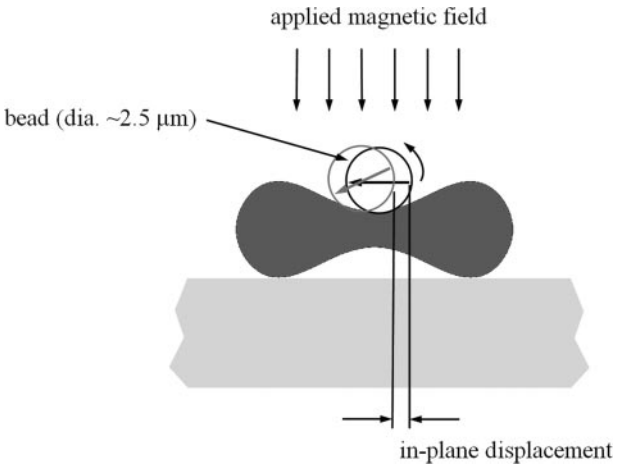


Fig. 2. Schematic of RBC optical magnetic twisting cytometry (OMTC) tests. A magnetic field is applied normal to the magnetization of the bead to generate a torque on the bound bead. The applied torque deforms the cell, which causes the bead to rotate and translate. The in-plane displacement of the bead is tracked optically.

sinusoidal forcing frequency was >4 Hz. Step functions had amplitudes between 1 and 4 G. The displacement response to the step functions was sampled at intervals of 50 ms.

*Measurement of the complex elastic modulus.* Two methods were used to extract the storage and loss moduli from the magnetic torque $T_s(t)$ and corresponding lateral bead motion $d(t)$. In the limit that the system becomes linear, these methods reduce to the same standard definitions for a linear viscoelastic system. The first method follows the approach of Fredberg and Stamenovic (21) for sinusoidal analysis of a nonlinear system and defines the apparent complex elastic moduli g* as

$$g^* = g' + ig'' \quad (2)$$

where $i^2 = -1$, $g'$ is the storage modulus, and $g''$ is the loss modulus. The modulus as defined here has raw measurement units of specific torque per unit lateral displacement, or Pa/nm, which do not depend on any model. However, these raw units can be converted to tradition material moduli using a model of membrane deformation, such as the one described below. The components of the complex modulus are determined from the limits of $T_s(t) - d(t)$ loop and the area, $A$, bounded by the $T_s(t) - d(t)$ loop, which represents the energy dissipation per cycle or hysteresis (Fig. 3). The phase angle $\phi$, loss tangent $\eta$, stiffness $g'$, and loss modulus $g''$ then become:

$$\phi = \sin^{-1}(4A/\pi\Delta T_s\Delta d) \quad (3)$$

$$g' = (\Delta T_s/\Delta d)\cos\phi \quad (4)$$

$$g'' = (\Delta T_s/\Delta d)\sin\phi = 4A/\pi\omega\Delta d^2 \quad (5)$$

where $\omega$ is the radian frequency. The second method used to extract the storage and loss modulus assumes the system is linear. The components of the complex elastic modulus are computed from the amplitudes of the applied torque, $\Delta T_s/2$, and displacement response, $\Delta d/2$, and the phase difference between the two signals $\phi$. The values of $\Delta T_s$, $\Delta d$, and $\phi$ were determined by fitting

$$T_s(t) = \frac{1}{2}\cdot\Delta T_s\cdot\sin(\omega t) \quad (6)$$

$$d(t) = \frac{1}{2}\cdot\Delta d\cdot\sin(\omega t + \phi) \quad (7)$$

to the experimental data. The loss and storage moduli were calculated using *Eqs. 4* and *5*, respectively.

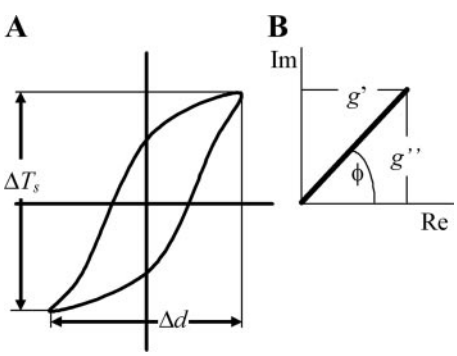


Fig. 3. *A*: "sigmoidal" hysteresis torque-displacement loop of a nonlinear system undergoing sinusoidal torque changes. The specific torque $T_s(t)$ is defined as the mechanical torque per unit bead volume and has dimensions of stress in Pascals. $T_s(t)$ is given by $T_s(t) = c\cdot H\cdot\cos\theta$, where $H$ is the magnetic twisting field in Gauss, $\theta$ is the angle of the bead's magnetic moment relative to the original magnetization direction, and $c$ is the bead constant, expressed as torque per unit bead volume per Gauss. In our case, $\theta \approx \pi/2$, hence $T_s(t)$ is proportional to the magnetic field [$T_s(t) = c\cdot H$]. *B*: stress in phase $g'$ (real) and out of phase $g''$ (imaginary) with bead displacement, expressed in complex plane. $\Delta d$, Bead displacement; Im, imaginary; Re, real; $\phi$, phase angle.

*Measurement of the creep response.* A step change in magnetic field was applied over 5 s, resulting in a lateral displacement of the bead. The responses on the rising and falling sides of the step signal were scaled from 0 to 1 for all experimental runs, and the arithmetic average over all runs was taken as the representative creep response.

*Computation of creep from measurements of the complex elastic modulus.* We measured the step response directly as described above, and also computed the step response from the Laplace transform of the response measured in the frequency domain. Let $J(t)$ be the creep response for unit step loading, and let $\tilde{J}(s)$ be its Laplace transform in variable $s$. Let $\tilde{G}(s)$ be the complex elastic modulus at complex frequency $s = i\omega$. The creep response and the complex modulus are related by

$$\tilde{J}(s) = 1/s\tilde{G}(s) \quad (8)$$

In RESULTS, we show that the real and imaginary parts of $\tilde{G}(i\omega)$ are described reasonably well by a power law in frequency with a constant offset. To satisfy the Kramers-Kronig relationship (3), this experimental observation implies that, in Laplace space, we have

$$\tilde{G}(s) = A + Bs^a \quad (9)$$

where $A$ and $B$ are parameters of the system, and $a$ is the power law exponent in frequency. Substituting *Eq. 9* in *Eq. 8*, it follows that

$$\tilde{J}(s) = 1/(As + Bs^{a+1}) \quad (10)$$

The creep response $J(t)$ is given by the inverse Laplace transform of *Eq. 10*. For general powers $a + 1$, there is no closed form expression for $J(t)$, and approximate methods are required. In particular, we must distinguish between the short time and the long time regimes. For short times ($t \to 0$), a Taylor expansion about $s = \infty$ and subsequent inversion suffices to yield

$$J(t) = \frac{t^a}{B\Gamma(a+1)} - \frac{At^{2a}}{B^2\Gamma(2a+1)} + \frac{A^2t^{3a}}{B^3\Gamma(3a+1)} - \dots \quad (11)$$

where $\Gamma(.)$ is the gamma function. This is a convergent power series for all $t$, but is useful only for small $t$, because the number of terms necessary for a good approximation rises extremely rapidly for large times. For long times, we perform a Taylor expansion about $s = 0$. The two leading terms and their inversion yield the asymptotic behavior of the creep response,

$$J(t) = \frac{1}{A} - \frac{Bt^{-a}}{A^2\Gamma(1-a)}, \quad t \to \infty \quad (12)$$

Note that this is the leading behavior of an asymptotic series; it is not convergent but does give the correct approach to the creep plateau. This two-term representation is valid only for $0 < a < 1$. The two limiting behaviors can then be joined by choice of a suitable intermediate time, below which *Eq. 11* is used, and larger than that for which *Eq. 12* is used. In our case, a sufficiently smooth transition between the two regimes is found for an intermediate time of ~0.024 s.

*FE modeling.* To approximate the deformation field induced in the RBC by magnetic bead twisting, we developed a FE model. Based on the geometry of the RBC (13), the cell membrane was meshed with 24,000 four-noded, bilinear, reduced-integration shell elements; its displacement was constrained such that the interior cell volume was constant. The membrane constitutive law was based on a strain energy potential used previously to model finite deformations of the RBC (8); in its application here, where the strains are small, this is essentially equivalent to a linear elastic two-dimensional (2D) membrane with given shear and bending ($B$) moduli. The boundary conditions imposed were as follows. The bottom surface of the RBC (interior to the lowermost circle of symmetry) was held fixed. The displacement of nodes adherent to the bead (bead nodes) were constrained to move in rigid translation or rotation with the bead, which was modeled as a

rigid solid. The tractions on all other nodes were set to zero. Although the net force applied to the bead was zero, a nonzero torque resulted in lateral (in-plane) displacement, with an apparent stiffness given by the ratio of the applied torque to the lateral displacement. A parametric study was performed to examine the effects of bending and shear moduli, as well as the degree of binding between the bead and the cell on the overall torque-displacement relationship measured in the experiments.

*Technical limitations.* Optical MTC is a tool that brings with it important technical advantages, such as the ability to probe the single cell with very small deformations and over wide ranges of time scale and amplitude. However, these advantages bring with them other technical limitations that can contribute to measurement variability. For example, the contact area between the cell and the bead, as well as the location at which the bead is attached to the cell, are not controlled and therefore vary from cell to cell. These shortcomings are mitigated to a large degree by the ability to measure a large number of cells and the ability to select cells in which the bead is centered. We found no significant correlation between bead location and stiffness, or cell size and stiffness. Moreover, the overall cell-to-cell variability was quite small.

Similarly, the FE analysis had several technical limitations. The nature of RBC viscoelasticity that we determined experimentally does not conform to any simple or known viscoelastic behavior and, as such, cannot be modeled from first principles. As such, we limited the FE analysis here to the purely elastic (i.e., static) case, but this is not a severe limitation, as it was observed that, over most of the experimental range, the loss modulus was much smaller than the storage modulus. We reasoned, therefore, that this model should provide *1*) a reasonable approximation of the deformation field induced by magnetic twisting, and specifically the extent to which the deformation is localized to the neighborhood of the bead; and *2*) a basis of comparison to previous static measurements of RBC deformability.

A second limitation is found in the specification of the membrane elastic properties. In the dimensional reduction of the real membrane to a 2D equivalent, we began with the assumption of isotropy and incompressibility. Such a material has only one elastic modulus, and, for a given thickness, the 2D equivalent shear modulus, area expansion modulus, and bending modulus are not independent but are fully determined. For material properties that approximate the 2D shear and bending moduli, this turns out to underestimate the area expansion modulus, and hence the apparent stiffness. However, since the response is *1*) significantly dominated by bending, as opposed to surface strain, and *2*) the area dilation is small compared with surface shear, this error is thought to be negligible.

## RESULTS

For a single cell with an applied sinusoidal field of 1 G, the displacement response was sinusoidal, and with increasing frequency the lag between the applied torque and the resulting displacement grew (Fig. 4). This increasing phase lag indicated greater dissipation at higher frequencies and was also reflected by the larger area enclosed by the displacement-torque loop. In contrast, the slope of the loop changed only at higher frequencies, indicating that the stiffness of the RBC changed little with frequency at frequencies <100 Hz (Fig. 4).

The apparent storage $g'$ and loss $g''$ moduli were calculated using two different approaches (MATERIALS AND METHODS) but yielded nearly the same results (Fig. 5). The only discrepancy between the approaches occurred at the very highest frequency (Fig. 5, *inset*), in which case the torque-displacement loop did not approximate an ellipse, and the first method (*Eqs. 3–5*) was thought to be preferable. Regardless of approach, cell stiffness $g'$ was insensitive to frequency up to 30 Hz, whereas the loss modulus $g''$ increased appreciably with increasing frequency $f$. A simple power law ($g'' \sim f^a$), with the exponent $a = 0.64$, fit $g''$ data reasonably well.

Loops remained elliptical, and the moduli remained independent of torque amplitude when the specific torque was <0.5

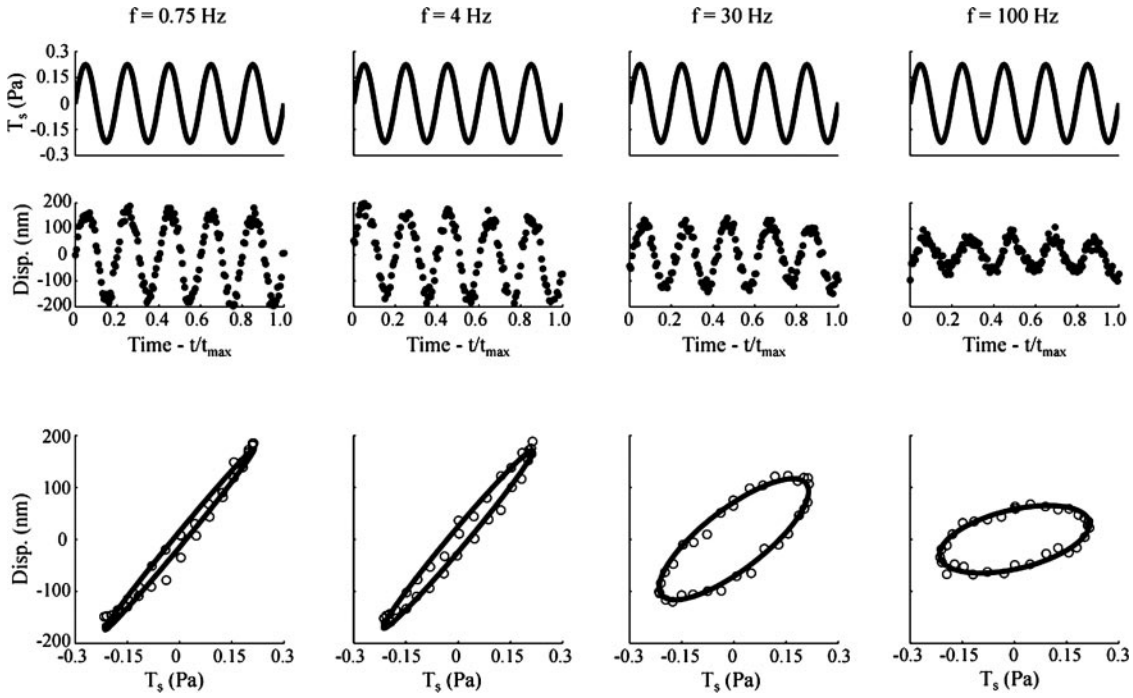


Fig. 4. RBC response to sinusoidal loading (0.75, 4, 30, and 100 Hz), applied specific torque $T_s$ as a function of time $t$ (*top* row); lateral displacement as a function of time $t$ (*middle* row), where $t_{max}$ is the duration of the 5 cycles; and displacement-torque loops for a representative bead at different frequencies (*bottom* row). Solid lines are fits to sinusoidal function to the displacement response. $f$, Frequency.

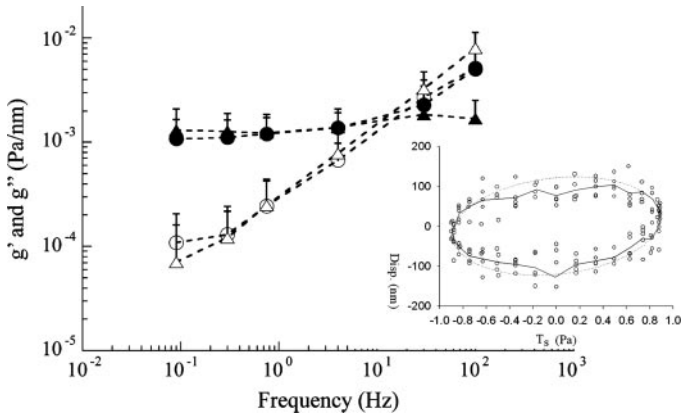


Fig. 5. Apparent storage g′ (solid symbols) and loss g″ (open symbols) moduli measured at frequencies from 0.1 to 100 Hz ($N = 48$). Data set *A* (circles) was extracted by calculating the limits and enclosed area of the torque displacement loops, while set *B* (triangles) shows the values extracted by fitting a sinusoidal function to the displacement response (see MATERIALS AND METHODS). Data plotted are means, and error bars represent 1 SD. *Inset*: displacement-specific torque loop for a representative bead at 100 Hz. Solid line is median data, and dashed line is fitted data to sinusoidal function of the bead displacement.

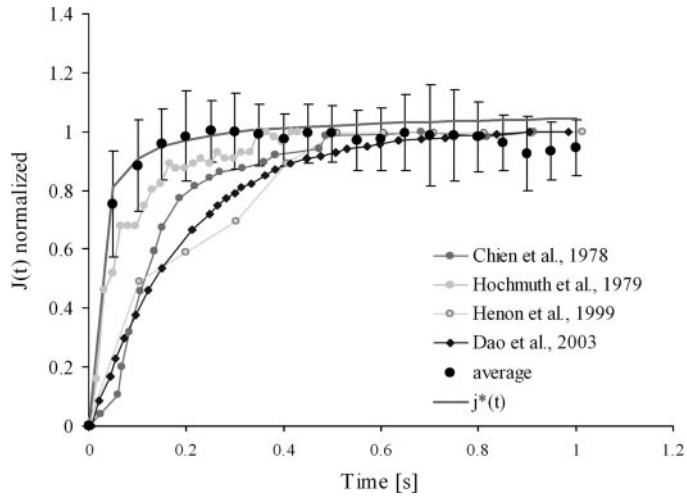


Fig. 7. Black data points are RBC responses, the normalized response to step loading ($N = 12$, means ± SD) (see MATERIALS AND METHODS). Gray solid line [$j^*(t)$] is the creep response computed from complex elastic modulus. Creep response data from previous studies are as follows: Chien et al. (5), dark gray circles; Hochmuth et at. (31), light gray circles; Henon et al. (28), black circles with gray center; and Dao et al. (8), black diamond, normalized by the last value or the data at 1 s.

Pa (Fig. 6). As the specific torque was increased, however, loops departed from an elliptical shape, and the hysteresis became load dependent, with larger dissipation occurring at higher specific torques. To quantify these nonlinearities, we computed the fundamental and higher harmonics of the bead displacement signal. Second and third harmonics were evident but small, accounting for 10% of the response at most. Similarly, g′ and g″ increased with increasing amplitude of the specific torque, suggesting slight strain hardening, but this trend did not reach statistical significance.

Within the linear range, the measured creep response function, $J(t)$, was in good agreement with the predictions based on *Eqs. 14* and *15* and measurements of the complex elastic modulus (Fig. 7). When the load was removed after a hold time of 5 s, the bead quickly returned to its original position, indicating full recovery. We found no difference between the deformation and the recovery phase.

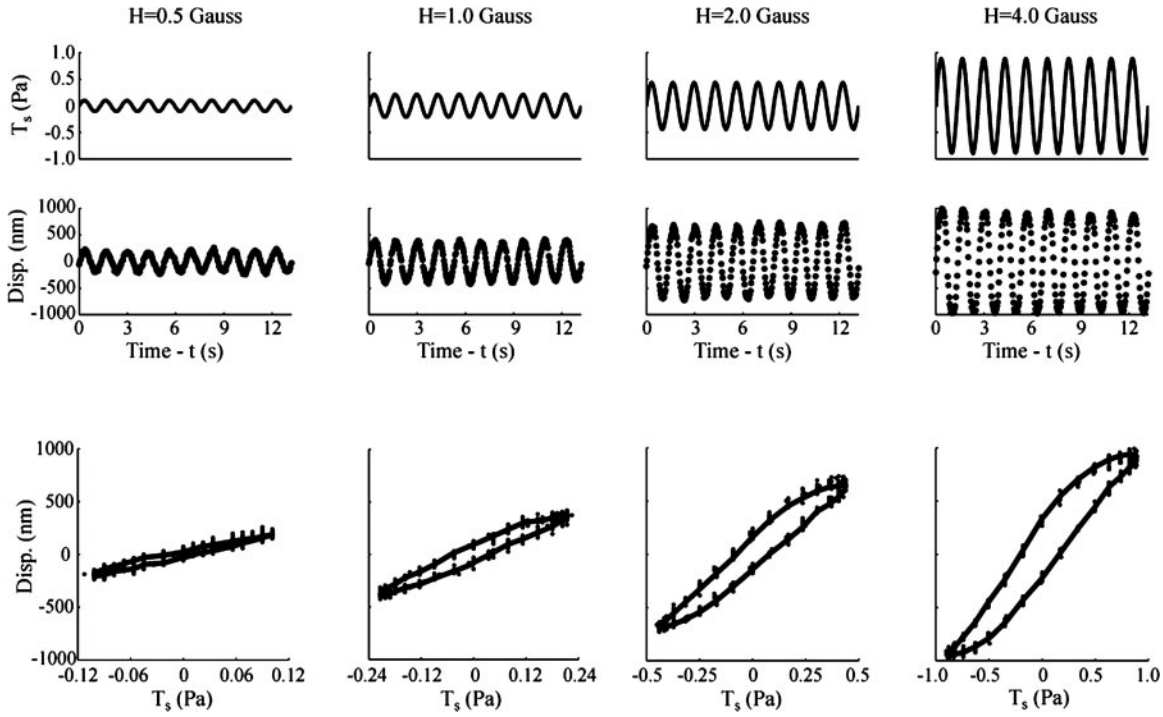


Fig. 6. RBC response to sinusoidal loading for tests with amplitudes of 0.5, 1, 2, and 4 G at a fixed frequency of 0.75 Hz, specific torque $T_s$ as a function of time *t* (*top* row), lateral displacement as a function of time *t* (*middle* row), and displacement-specific torque $T_s$ loops for a representative bead at different amplitudes (*bottom* row). Solid lines are median data. *H*, applied magnetic twisting field.

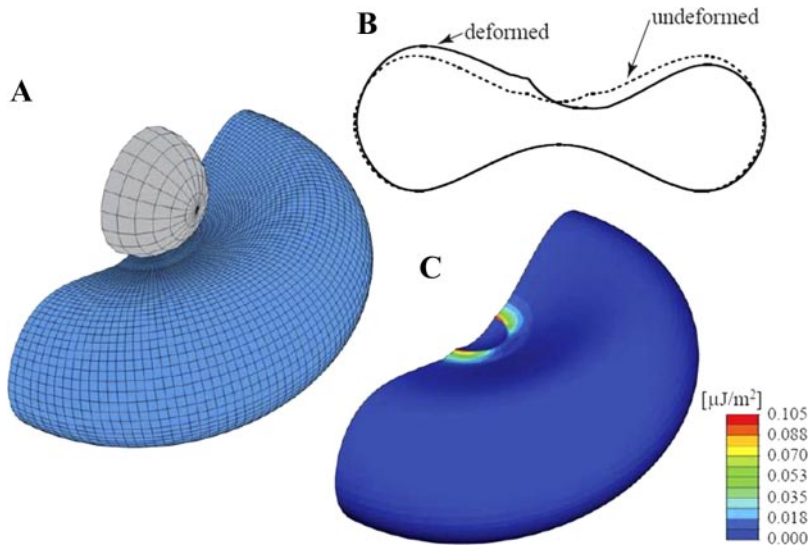


Fig. 8. *A*: finite element (FE) mesh used for mechanical simulations of the OMTC RBC test. Symmetry is used, such that the model consists of only one-half of the cell. *B*: the un-deformed and deformed shape predicted by the FE model of cell on the symmetry plane. The displacements have been magnified by a factor of four. *C*: plot of the elastic strain energy density across the entire cell (the bead has been removed for clarity).

RBC deformations predicted by the FE simulation are shown in Fig. 8, where displacement has been increased by fourfold for clarity. Wall displacements spanned the entire cell (Fig. 8*B*), but the strain energy density was much more localized (Fig. 8*C*). To characterize the distribution of elastic strain energy, we used the first moment of the strain energy density distribution with respect to arc length along the cut surface in Fig. 8*C*, with radial weighting appropriate to cylindrical coordinates. This characteristic length was ~2.5 times the contact radius, thus showing that elastic strain energy density is modestly localized to the neighborhood of the bead.

Bending dominated in the vicinity of the bead, but surface strain dominated far from the bead. However, in terms of the total energy of cell deformation, bending was the larger contributor. When the FE simulations were performed for a range of bending moduli (0.2–0.8 pN-μm) and shear moduli (6–12 pN/μm), which span previous measurements under static conditions with MA and OT (8, 16), the apparent stiffness was consistent with our measurements at low frequencies (Fig. 9). A 10% increase in the bending modulus resulted in a 7% increase in the apparent stiffness, whereas a 10% increase in the shear modulus resulted in only a 3% increase in the apparent stiffness. While both factors were important, bending was predominant.

## DISCUSSION

Here we report the complex viscoelastic properties of the isolated RBC. Our principal findings are a linear range in which elastic stresses were independent of frequency and were much large than frictional stresses, except at very high frequencies. Frictional stresses depended on frequency, but not as predicted by any simple viscoelastic model. In the remainder of this section, we begin by addressing the nonlinearities that arise at large deformations. We then limit attention to the linear range of responses and contrast these results with those previously reported in the literature from measurements using MA, OT, and ED. We conclude by commenting on the suitability of

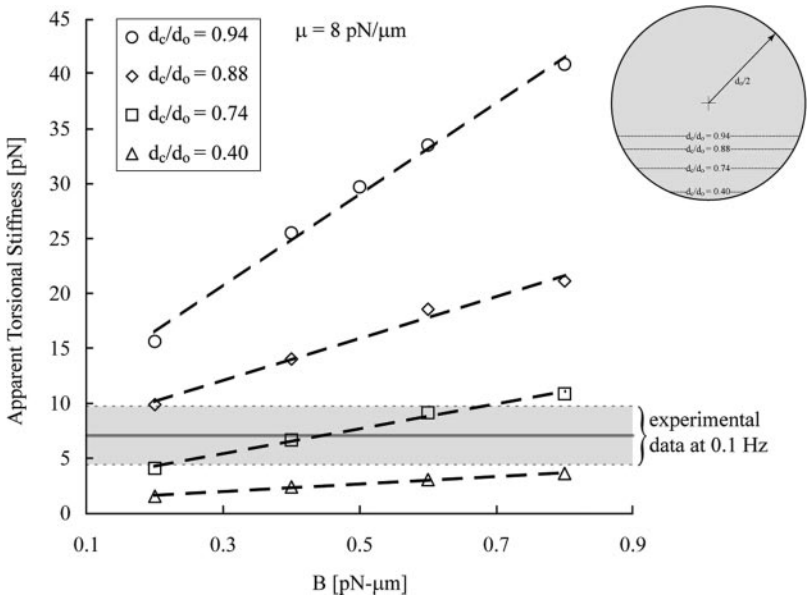


Fig. 9. The apparent torsional stiffness (i.e., applied torque divided by bead displacement) as a function of bending moduli, *B*, and contact diameters for a fixed value of shear modulus μ. The measured apparent torsional stiffness at 0.1 Hz is shown for comparison (solid line shows mean value, and gray region indicates mean ± 1 SD). $d_c$, diameter of the bead contact to the cell; $d_o$, diameter of bead.

models that have been used in the past to interpret deformability of the RBC.

For smaller torque amplitudes, the torque-displacement loops were nearly elliptical, and harmonics were small (Fig. 6), but, for larger applied torques, nonelliptical loops were observed, and harmonics became more pronounced (Fig. 6). Such behavior represents evidence of small strain-hardening nonlinear responses. Potential factors leading to these nonlinearities are, first, geometrical. The torque applied to the bead varies as the cosine of the angle between the magnetization and the applied field (*Eq. 1*); if the bead pivoted around a contact point at the bead perimeter, this effect would result in errors of no more than 10% for large bead rotations ($\theta < 26°$) or lateral bead displacements ($d < 570$ nm). Another geometrical factor that may contribute is the large deformations of the thin shell structure of the cell. The deformation of the shell structure is complex (Fig. 8), and one would expect that, when the deformations become large, the change in geometry will result in a nonlinear relationship between the applied load and displacement. Other possible factors for the observed nonlinear behavior are related to the intrinsic material properties of the cell membrane itself. In this context, OT tests have demonstrated that the effective shear modulus of the red cell membrane increases dramatically at large deformations (8, 36). In the studies reported here, we saw a linear range followed by slight strain hardening, but no evidence of strain softening or yielding. In the remainder of the DISCUSSION, we restrict attention to experiments in which deformations were small and the response was linear.

Direct measurement of the creep function (Fig. 7, black data points) compared favorably with that computed from direct measurements of the complex modulus (Fig. 7, gray solid line), suggesting that, when the torque amplitude is small, a linear response function in either the time or Fourier domain is sufficient to characterize the rheological properties of the RBC. Moreover, by transforming data from the Fourier domain (Fig. 5) into the time domain (Fig. 7, gray solid line), we were able to compare our observations to step responses of the RBC reported previously in the literature (Fig. 7). Compared with previous measurements, our direct measurements were close to those reported by Hochmuth et al. (31) (Fig. 7, light gray circles), but somewhat faster than those reported by the others. One possible explanation for these differences may be associated with differences in loading. By the nature of our bead twisting protocol, the applied torque and induced rotation vectors lie in the plane of the apical surface of the cell, which, in turn, implies that the loading is supported by both shear and bending, but predominantly by bending of the membrane. To the extent that simple bending is associated with less dissipation than loadings involving isotropic membrane tension and associated 2D bulk dilation, or normal stress gradients associated with bulk three-dimensional transport of intracellular material, responses might be more rapid. The idea that bending stiffness is important in this context is supported by the observation of a parallel elastic behavior as seen especially in the low-frequency regime in Fig. 5 (and as modeled by *Eq. 9*) and is supported by the FE simulations, which correspond to low-frequency regime.

Creep and relaxation responses, such as those shown in Fig. 7, have been conventionally modeled as a function of time with an exponential decay (14–16). That is to say, all previous models of RBC dynamics are based on the assumption that dynamic responses can be characterized by one or a few characteristic relaxation times. While some studies [e.g., Dao et al. (8), diamond points in Fig. 7] report good agreement with an exponential behavior, virtually none of these have followed the response over a time course that is sufficiently long to distinguish between exponential behavior vs. other possibilities [e.g., Hochmuth et al. (31) (Fig. 7, gray circles) and Henon et al. (28) (Fig. 7, black circle with gray center)]. Nonetheless, all of these studies used single exponentials to characterize the first 300–400 ms and, for MA and ED, and OT experiments, respectively, have suggested time constants of 0.10–0.13 s and 0.13–0.25 s (12, 36). By contrast, data reported here firmly establish that, in the case of MTC, at least, the dynamic response of the RBC exhibits no distinct time constants. Rather, the dynamic response follows a power law decay. We cannot rule out that MTC yields power law response, whereas MA, OT, and ED tests probe different facets of RBC dynamics and yield responses that conform to an exponential decay. Alternatively, we propose here that relaxation times estimated previously from data, and any models that rest upon them, are artifactual. This is not to say that the estimated value of a time constant is inaccurate, but rather to say that, in such a system, the very concept of a time constant is meaningless (49). The artifact, we suggest, arises from forcing an exponential fit to data of limited temporal duration that, in actuality, defines a power law response (49).

In connection with power law responses, the frequency dependence of the elastic and frictional moduli (Figs. 5 and 6) of the RBC differed dramatically from that of spread adherent somatic cells, such as smooth muscle cells, fibroblasts, and epithelial cells, that have been measured using the same technique (19, 32, 40) and other techniques (1, 9, 10, 43). In a variety of adherent cell types, measurements of $g'$ and $g''$ vs. frequency typically exhibit weak power law behaviors, with a viscous Newtonian contribution arising only at very high frequencies. By contrast, $g'$ of the RBC was nearly independent of frequency up to 30 Hz (Fig. 6), and $g''$ increased with frequency as a power law throughout the measurement range, but the exponent (0.64) was much greater than that seen in somatic cells, but systematically weaker than expected for a Newtonian fluid. The frequency dependence of $g'$ and $g''$ observed in RBCs (Figs. 5 and 6) also differed from that measured in in vitro systems, such as cross-linked actin gels (23, 46, 50).

What factors might account for the frequency dependence of $g'$ and $g''$? The RBC membrane has an outer phospholipid bilayer attached to an inner 2D cytoskeleton network (2, 24, 25, 34). The links of the network consist of flexible spectrin molecules ($R \sim 80$–$100$ nm), cross-linked at the network nodes by a complex containing a short (30 nm) actin filament, band-4.1, and other proteins (2, 45). The spectrin cytoskeleton of RBC is slightly stretched and under tension, even in the un-deformed state (20, 51). We speculate that, on the one hand, the 2D spectrin prestressed network is probably responsible for the elastic-like response and the apparent storage moduli being insensitive to frequency. On the other hand, the origin of the power law behavior of $g''$ is uncertain. However, the membrane is thought to be the dominant source of viscous dissipation, because the membrane viscous dissipation is two orders of magnitude greater than that in the internal hemoglobin solution

(14, 30). Moreover, hemoglobin solutions behave like Newtonian fluids (7), and so the RBC intracellular milieu is unlikely to yield the non-Newtonian behavior we find in g″.

Interlayer coupling of the lipid bilayer (17), including the potential effects of lipid "flip-flop" (41), has been proposed as a candidate for viscous loss mechanisms, especially in circumstances where membrane curvature is rapidly changing. It is unlikely that the global effect of transmission of cumulative tension and associated area expansion is responsible, however, since our bead movements are more localized compared with, for example, vesicle tethering phenomena. Nevertheless, the interlayer coupling of the bilayer immediately bound to the surface of the bead in our experiments remains a potential source of dissipation, despite uncertainty regarding its frequency-dependent behavior.

Lipid bilayer fluctuations driven by thermal forces are also a potential loss mechanism (25, 52). On the one hand, Gov's theoretical analyses are based on a model that replaces the spectrin network with a rigid shell separated from the bilayer, but with an induced effective surface tension and harmonic potential. As our beads are firmly attached to the spectrin network, it is unclear that bilayer fluctuations taken over a rigid cytoskeleton, even with equivalent bilayer mechanics, will capture the features of the dissipation we observe. On the other hand, all approaches that relate spontaneous fluctuation phenomena directly to dissipation seen in driven motion rely on some form of the fluctuation-dissipation theorem (FDT). FDT is strictly valid only in systems at thermodynamic equilibrium and is known to be strongly violated in other cell types (4).

To our knowledge, length scales and time scales over which FDT might hold for the RBC are unknown. If FDT does hold, then the anomalous frequency dependence of $f^{-5/3}$ predicted by Gov et al. (25) for the mean square normal displacement in Fourier space would translate into $f^{2/3}$ for the frequency dependence of g″, which is close to the behavior that we observe (Fig. 5). This coincidence of predicted vs. measured exponents points to the importance of future studies to examine systematically the prefactor, which may then elucidate whether spontaneous fluctuations of the lipid bilayer may be linked to the dissipation observe for driven deformations measured with beads firmly connected to the spectrin network.

Spectrin network fluctuations driven by metabolic and thermal sources (26, 33, 47) can also be a candidate for viscous loss mechanism, although the sources are found to be important only at low frequencies (44). At high frequencies, it has been shown that fluctuations in semiflexible polymers driven by thermal forces leads to viscoelasticity that scales with frequency with a universal exponent of 3/4 (9, 22, 38), a behavior that is not observed in experiments reported here. Nevertheless, interlayer coupling, bilayer fluctuations, and spectrin fluctuations remain candidates and potential mechanisms that can lead to the observed viscous dissipation.

*Conclusions.* Here we have reported elastic and frictional moduli of the isolated RBC over a wide range of forcing time scale and forcing amplitude. Except at very high frequencies, elastic stresses dominated and were independent of frequency. Frictional stresses depended on frequency but not as predicted by any simple model. This frictional behavior was non-Newtonian and suggests origins different than surface viscosity of lipid membrane components or the viscous hemoglobin solution (14, 15, 30). It is unclear if the frequency dependence of g″ is related to membrane molecular fluctuations or metabolic activity controlled by intracellular concentrations of ATP (25, 26, 47). Further exploration of these processes could shed light on the underlying viscoelastic deformation characteristics of the RBC. Most important, the data reported here indicate that a power-law fluid taken in parallel with a Hookean stiffness is an appropriate phenomenological model to describe dynamic responses of the RBC in the linear range.

## ACKNOWLEDGMENTS

We thank Rebecca Stearns for helping with the electron microscopy, P. N. Tang for assisting in the experiments and simulations, and Emil Millet for producing ferrimagnetic microbeads.

## GRANTS

J. J. Fredberg acknowledges support from the National Institutes of Health (NIH) Grants HL33009, HL65960, and HL59682. S. Suresh acknowledges support from the NIH/National Institute of General Medical Sciences Grant 1-R01-GM076689-01, and the Advanced Materials for Micro and NanoSystems Program and the Computational Systems Biology Program of the Singapore-MIT Alliance.

## REFERENCES

1. **Alcaraz J, Buscemi L, Grabulosa M, Trepat X, Fabry B, Farre R, Navajas D.** Microrheology of human lung epithelial cells measured by atomic force microscopy. *Biophys J* 84: 2071–2079, 2003.
2. **Bennett V.** The spectrin-actin junction of erythrocyte membrane skeletons. *Biochim Biophys Acta* 988: 107–121, 1989.
3. **Booij HC, Thoone G.** Generalization Of Kramers-Kronig transforms and some approximations of relations between viscoelastic quantities. *Rheologica Acta* 21: 15–24, 1982.
4. **Bursac P, Lenormand G, Fabry B, Oliver M, Weitz DA, Viasnoff V, Butler JP, Fredberg JJ.** Cytoskeletal remodelling and slow dynamics in the living cell. *Nat Mater* 4: 557–561, 2005.
5. **Chien S, Sung KL, Skalak R, Usami S, Tozeren A.** Theoretical and experimental studies on viscoelastic properties of erythrocyte membrane. *Biophys J* 24: 463–487, 1978.
6. **Chien S, Sung KLP, Skalak R, Usami S.** Theoretical and experimental studies on viscoelastic properties erythrocyte-membrane. *Biophys J* 24: 463–487, 1978.
7. **Cokelet GR, Meiselman HJ.** Rheological comparison of hemoglobin solutions and erythrocyte suspensions. *Science* 162: 275–277, 1968.
8. **Dao M, Lim CT, Suresh S.** Mechanics of the human red blood cell deformed by optical tweezers. *J Mech Phys Solids* 51: 2226–2280, 2003.
9. **Deng L, Trepat X, Butler JP, Millet E, Morgan KG, Weitz DA, Fredberg JJ.** Fast and slow dynamics of the cytoskeleton. *Nat Mater* 5: 636–640, 2006.
10. **Desprat N, Richert A, Simeon J, Asnacios A.** Creep function of a single living cell. *Biophys J* 88: 2224–2233, 2005.
11. **Drochon A.** Rheology of dilute suspensions of red blood cells: experimental and theoretical approaches. *European Physical Journal-Applied Physics* 22: 155–162, 2003.
12. **Engelhardt H, Sackmann E.** On the measurement of shear elastic moduli and viscosities of erythrocyte plasma membranes by transient deformation in high frequency electric fields. *Biophys J* 54: 495–508, 1988.
13. **Evans E, Fung YC.** Improved measurements of the erythrocyte geometry. *Microvasc Res* 4: 335–347, 1972.
14. **Evans EA, Hochmuth RM.** Membrane viscoelasticity. *Biophys J* 16: 1–11, 1976.
15. **Evans EA, Hochmuth RM.** Membrane viscoplastic flow. *Biophys J* 16: 13–26, 1976.
16. **Evans EA, Skalak R.** *Mechanics and Thermodynamics of Biomembranes*. Boca Raton, FL: CRC, 1980.
17. **Evans EA, Yeung A.** Hidden dynamics in rapid changes of bilayer shape. *Chem Phys Lipids* 73: 39–56, 1994.
18. **Fabry B, Maksym GN, Butler JP, Glogauer M, Navajas D, Taback NA, Millet EJ, Fredberg JJ.** Time scale and other invariants of integrative mechanical behavior in living cells. *Phys Rev E Stat Nonlin Soft Matter Phys* 68: 041914, 2003.
19. **Fabry B, Maksym GN, Shore SA, Moore PE, Panettieri RA Jr, Butler JP, Fredberg JJ.** Selected contribution: Time course and heterogeneity of

contractile responses in cultured human airway smooth muscle cells. *J Appl Physiol* 91: 986–994, 2001.
20. **Fournier JB, Lacoste D, Raphael E.** Fluctuation spectrum of fluid membranes coupled to an elastic meshwork: jump of the effective surface tension at the mesh size. *Phys Rev Lett* 92: 018102, 2004.
21. **Fredberg JJ, Stamenovic D.** On the imperfect elasticity of lung tissue. *J Appl Physiol* 67: 2408–2419, 1989.
22. **Gittes F, Schnurr B, Olmsted PD, MacKintosh FC, Schmidt CF.** Microscopic viscoelasticity: shear moduli of soft materials determined from thermal fluctuations. *Phys Rev Lett* 79: 3286–3289, 1997.
23. **Goldmann WH, Tempel M, Sprenger I, Isenberg G, Ezzell RM.** Viscoelasticity of actin-gelsolin networks in the presence of filamin. *Eur J Biochem* 246: 373–379, 1997.
24. **Gov N.** Membrane undulations driven by force fluctuations of active proteins. *Phys Rev Lett* 93: 268104, 2004.
25. **Gov N, Zilman AG, Safran S.** Cytoskeleton confinement and tension of red blood cell membranes. *Phys Rev Lett* 90: 228101, 2003.
26. **Gov NS, Safran SA.** Red blood cell membrane fluctuations and shape controlled by ATP-induced cytoskeletal defects. *Biophys J* 88: 1859–1874, 2005.
27. **Hategan A, Sengupta K, Kahn S, Sackmann E, Discher DE.** Topographical pattern dynamics in passive adhesion of cell membranes. *Biophys J* 87: 3547–3560, 2004.
28. **Henon S, Lenormand G, Richert A, Gallet F.** A new determination of the shear modulus of the human erythrocyte membrane using optical tweezers. *Biophys J* 76: 1145–1151, 1999.
29. **Hochmuth RM, Evans EA, Colvard DF.** Viscosity of human red cell membrane in plastic flow. *Microvasc Res* 11: 155–159, 1976.
30. **Hochmuth RM, Waugh RE.** Erythrocyte membrane elasticity and viscosity. *Annu Rev Physiol* 49: 209–219, 1987.
31. **Hochmuth RM, Worthy PR, Evans EA.** Red cell extensional recovery and the determination of membrane viscosity. *Biophys J* 26: 101–114, 1979.
32. **Laudadio RE, Millet EJ, Fabry B, An SS, Butler JP, Fredberg JJ.** Rat airway smooth muscle cell during actin modulation: rheology and glassy dynamics. *Am J Physiol Cell Physiol* 289: C1388–C1395, 2005.
33. **Lee JC, Discher DE.** Deformation-enhanced fluctuations of the erythrocyte's spectrin-actin nodes and relation to single molecule measures of spectrin unfolding. *Cell Mol Biol Lett* 6: 217, 2001.
34. **Li J, Dao M, Lim CT, Suresh S.** Spectrin-level modeling of the cytoskeleton and optical tweezers stretching of the erythrocyte. *Biophys J* 88: 3707–3719, 2005.
35. **Miller LH, Baruch DI, Marsh K, Doumbo OK.** The pathogenic basis of malaria. *Nature* 415: 673–679, 2002.
36. **Mills JP, Qie L, Dao M, Lim CT, Suresh S.** Nonlinear elastic and viscoelastic deformation of the human red blood cell with optical tweezers. *Mech Chem Biosyst* 1: 169–180, 2004.
37. **Mohandas N, Evans E.** Mechanical properties of the red cell membrane in relation to molecular structure and genetic defects. *Annu Rev Biophys Biomol Struct* 23: 787–818, 1994.
38. **Morse DC.** Viscoelasticity of concentrated isotropic solutions of semiflexible polymers. 2. Linear response. *Macromolecules* 31: 7044–7067, 1998.
39. **Platt OS.** The sickle syndrome. In: *Blood: Principles and Practice of Hematology*, edited by Haldin RI, Lux SE, Stossel TP. Philadelphia, PA: Lippincott, 1995, p. 1592–1700.
40. **Puig-de-Morales M, Millet E, Fabry B, Navajas D, Wang N, Butler JP, Fredberg JJ.** Cytoskeletal mechanics in adherent human airway smooth muscle cells: probe specificity and scaling of protein-protein dynamics. *Am J Physiol Cell Physiol* 287: C643–C654, 2004.
41. **Raphael RM, Waugh RE, Svetina S, Zeks B.** Fractional occurrence of defects in membranes and mechanically driven interleaflet phospholipid transport. *Phys Rev E Stat Nonlin Soft Matter Phys* 64: 051913, 2001.
42. **Riquelme BD, Valverde J, Rasia RJ.** Complex viscoelasticity of normal and lectin treated erythrocytes using laser diffractometry. *Biorheology* 35: 325–334, 1998.
43. **Smith BA, Tolloczko B, Martin JG, Grutter P.** Probing the viscoelastic behavior of cultured airway smooth muscle cells with atomic force microscopy: stiffening induced by contractile agonist. *Biophys J* 88: 2994–3007, 2005.
44. **Suresh S, Spatz J, Mills JP, Micoulet A, Dao M, Lim CT, Beil M, Sefferlein T.** Connections between single-cell biomechanics and human disease states: gastrointestinal cancer and malaria. *Acta Biomater* 1: 15–30, 2005.
45. **Takakuwa Y.** Regulation of red cell membrane protein interactions: implications for red cell function. *Curr Opin Hematol* 8: 80–84, 2001.
46. **Tseng Y, An KM, Esue O, Wirtz D.** The bimodal role of filamin in controlling the architecture and mechanics of F-actin networks. *J Biol Chem* 279: 1819–1826, 2004.
47. **Tuvia S, Levin S, Bitler A, Korenstein R.** Mechanical fluctuations of the membrane-skeleton are dependent on F-actin ATPase in human erythrocytes. *J Cell Biol* 141: 1551–1561, 1998.
48. **Valberg PA, Butler JP.** Magnetic particle motions within living cells. Physical theory and techniques. *Biophys J* 52: 537–550, 1987.
49. **Wilson TA.** Time constants may be meaningless in exponentials fit to pressure relaxation data. *J Appl Physiol* 77: 1570–1571, 1994.
50. **Zaner KS.** The effect of the 540-kilodalton actin cross-linking protein, actin-binding protein, on the mechanical properties of F-actin. *J Biol Chem* 261: 7615–7620, 1986.
51. **Zeman K, Engelhard H, Sackmann E.** Bending undulations and elasticity of the erythrocyte membrane: effects of cell shape and membrane organization. *Eur Biophys J* 18: 203–219, 1990.
52. **Zilman AG, Granek R.** Membrane dynamics and structure factor. *Chem Phys* 284: 195–204, 2002.